Effect of SnO addition on structure and properties of P_2O_5-SnF_2-WO_3-B_2O_3 glasses for low temperature sealing

JINLONG DIAO[a,b], XIN XU[c], DONGWEI ZHANG[a,b], TAO ZHENG[a,b,*], ZHENGYU LI[a], JINGWEN LV[a]
[a]*School of Materials and Science Engineering, Changchun University of Science and Technology, Changchun, China*
[b]*Jilin Provincial Science and Technology Innovation Center of Optical Materials and Chemistry, Changchun University of Science and Technology, Changchun, China*
[c]*Basic Department, Aviation University of Air Force, Changchun, China*

Phosphate-tinfluoride-tungsten-boron oxide (P_2O_5-SnF_2-WO_3-B_2O_3, PSWB) glasses were prepared for low-temperature sealant materials using the conventional melt-quenching technology. In these glasses SnF_2 was partially replaced with SnO. The effect of SnO concentration on glass structure and properties were investigated. Full characterizations have been carried out by XRD, TEC, SEM, DSC, as well as FTIR. As revealed from glass density and electrical resistance, the parameters increase almost linearly with the addition of SnO. The infrared spectra reflect that there is an increasing number of Sn-O-P and P-O-P, as the SnO concentration rises from 0 to 25 wt %. Besides, changes in curves of thermal expansion indicate that the increasing SnO content diminishes the coefficient of thermal expansion and promote the improvement of the glass transition and softening temperature. For the immersing measurements, the SEM analysis implies that the glass water durability has been improved as the SnO concentration increases. Revealed from the DSC results, the molten temperature of the glass is near 300 ^oC, and glass powder in the remelt test exhibits sufficient flowability, which provides new ideas for the development of low temperature and environmentally friendly sealant materials.

(Received May 20, 2019; accepted December 10, 2019)

Keywords: Low temperature sealing, Phosphate glass, Network structure, Water durability

1. Introduction

Lead-containing glasses have been dominant in the low- temperature sealant materials for years. The lead-containing glasses are restricted in commercial use due to environmental protection [1]. Currently, the phosphate glass has drawn much attention of researchers for its unique advantages, such as lead-free, low melting temperature, and adjustable coefficient of thermal expansion (*CTE*) [2-4]. Thus, the phosphate glass has been used as sealant materials of vacuum glazing brazing joints, PDP substrate and the like [5-7]. However, poor chemical stability limits its wider application. The phosphate glasses mainly consist of [PO_4] tetrahedrons, whose structure is irregular because of the different P=O and P-O bond length [8]. Besides that, it has been proved that the P=O is easily destroyed by the H^+ from water, forming the P-OH [9-10].

Still, many efforts have been taken to improve the chemical stability of phosphate glasses. Studies mainly concentrate on investigating the properties optimization of phosphate glasses by addition of trivalent and transition metal ions, like Fe^{3+}, Al^{3+}, Cu^{2+} and others [11-13]. Moreover, phosphate glass-ceramic is a heated topic. Venkateswara et al. [14] reported that silicon nitride can be added to enhance the water durability of phosphate glass. On the other hand, the joining temperature tends to be lower for protecting the devices. Unfortunately, the addition of Na^+, K^+ can reduce the degree of polymerization of glass [15], which allows a decrease in the transition temperature of phosphate glass, while a potential pitfall is that the ion exchange will be accelerated. This signifies the phosphate glass containing alkali metal ions may be insufficient on resisting the moisture erosion in some humid environment [16]. Under the circumstance, it is contradictory to maintain synchronously the low melting property and good chemical stability.

Tin-fluorophosphate glass was first reported by Tick in 1984 [17]; he claimed that the tin oxide played a crucial role in shrinking the melting point of phosphate glass, the Sn was not only a network modifier but a glass former within the phosphate glass system [18,19]. To the best of our knowledge, no reports are focused on the P_2O_5-SnF_2-WO_3 system. Herein, the SnO as the second source of tin is added into the pristine glass with a composition of $30P_2O_5$-$50SnF_2$-$15WO_3$-$5B_2O_3$, for investigating its influence on the glass structure and

properties. The results show that the addition of SnO is effective in tuning the thermal properties, water durability and resistivity of the phosphate glass.

2. Experiment and analysis

Glass samples with $30P_2O_5$-$(50-x)SnF_2$-$xSnO$-$15WO_3$-$5B_2O_3$ composition were prepared using the melting quenching method; the samples were marked as A1 to A6. A hundred grams raw materials of reagent grade $NH_4H_2PO_4$, SnF_2, SnO, WO_3, H_3BO_3 were weighed and mixed in an agate mortar for minutes. The mixture was melt in platinum crucible at 450 ^oC for 1 hour. Then they were quenched on stainless plates. The samples were annealed in a 100 ^oC muffle for 2 hours.

The phase composition of sample was studied using the X-ray diffraction (XRD), (Cu Kα radiation, PAN analytical X'Pert PRO diffractometer, Netherlands). Glass thermal expansion curves (TEC) were determined by the DIL402PC (NETZSCH, Germany) with a heating rate of 5 ℃/min. The transition temperature (T_g) of glass is the temperature at which glass changes from amorphous solid to molten state. Diametric temperature (T_f) is the temperature at which the glass viscosity can no longer support the rigid shape of glass, resulting in deformation. Both T_g and T_f can be obtained from the thermal expansion curve. The density of glass was measured by the HYDMDB-Ⅱ (YOUHONG, Shanghai, China) using Archimedes method in distilled water; samples for each composition were tested for three times to get average value. The electrical resistance was investigated at the voltage of 1000 V by the digital high resistance measuring instrument (EST-121, BMILP, China). The glass was cut into a bulk shape of 20 mm*20 mm*15 mm and was polished.

To discuss the network structure, FTIR spectroscopy was performed using the infrared spectrometer in the range of 400–4000 cm^{-1} at room temperature (FT/IR-550, JASCO, Japan). The KBr technique was employed, and the mixture of the glass powder (20 mg) and highly purity KBr powder (200 mg) was pressed into thin pellets for the test. Under a humid environment of 90 ^oC distilled water for 48 hours, the mass loss of glass was used to reveal the water durability. The glass was cut into a bulk shape of 10 mm*10 mm*5 mm and was polished. For further analysis, the micro- structure of the glass surface after immersing was investigated by the SEM (JSM-6701F, JEOL, Japan). Ten grams glass powder was pressed in a cylinder shape in a stainless steel mould. The powder cylinder was melted in a muffle from room temperature with a heating rate of 10 ^oC/min.

3. Results and discussion

3.1. Glass structure

3.1.1. XRD

The phase states of SnO samples were studied The X-ray diffractograms of 0-25 wt% SnO-containing glasses in comparison with the PSWB parent glass samples are shown in Fig. 1. The broad humps appearing in the XRD patterns confirm the amorphous nature of all the glass samples. Besides that, the large board peak center is observed at around $2\theta=25^o$, which is a typical character of phosphate glass [21, 22].

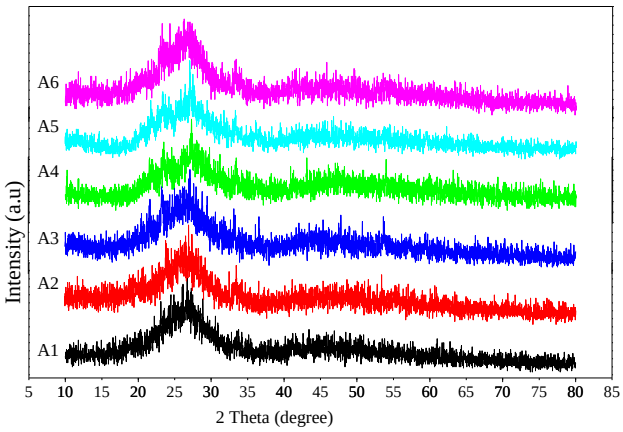

Fig. 1. The XRD of $30P_2O_5$-$(50-x)SnF_2$-$xSnO$-$15WO_3$-$5B_2O_3$ glasses

3.1.2. Infrared spectra

The infrared transmittance spectra in the range 400 to 4000 cm^{-1} of the PSWB glass are shown in Fig. 2. Bands and their assigned stretching modes have been discussed. Bands at about 450 cm^{-1} are related to the B-O bending vibration in [BO_3] units. Bands centered at 540 cm^{-1} are associated with the P-O asymmetrical stretching vibration (non-bridging oxygen, NBO). The NBO is generally connected by the strong polarization from Sn (IV) and W (VI) in PSWB glass. The bands located at about 750 cm^{-1} are assigned to the bridging oxygen stretching modes, which are consisted of P-O-P linkage. The intensity is observed to have a slight increase with the addition of SnO, and the band shape becomes broader with more SnO content. There is an increase in the O/P ratio as the SnO comes to replace the SnF_2. As revealed from the survey of Cordeiro et al. [23], the fluoride anion has a strongly breaking effect on P-O-P linkage, shorts the phosphate chains and generates terminal bonds like P-F and Sn-F bonds. The oxygen is more likely to play a non-bridging role within the glass's lack of SnO. Under the circumstance, the connection is not enough between the central atom like P, Sn, even B, which consequently leads to a loose glass structure.

Increasement in O/P ratio provides more bridging oxygens, which would be beneficial to enhance glass structure. Comparing to the frail P-O-P linkage under fluoride, the Sn-O-Sn linkage has priority on stability. The broad bands near 1250 cm^{-1} are related to the bending vibration of O-P in the P=O double bonds [24]. With the increase of SnO content, the frequency of P=O moves to lower wavenumbers. Among the materials available [25, 26], if there is not enough oxygen to act as bridging oxygen, P and O are more likely to form P=O л bonds. A considerable number of P=O bonds will lead to a low degree of cross-linking of network structure, which makes it difficult to transform into a three-dimensional frame structure. The forceful bands at about 1620 cm^{-1} are related to the O-H bending vibration [27], which belongs to the structural water of glass. According to the research of Ignatieva et al. [28], the P=O bonds are easily destroyed by H_2O in a humid environment, generating the P-OH. Notably, its intensity is significant in the glass with a low SnO component, and the band becomes narrower as the SnO content increases [31].

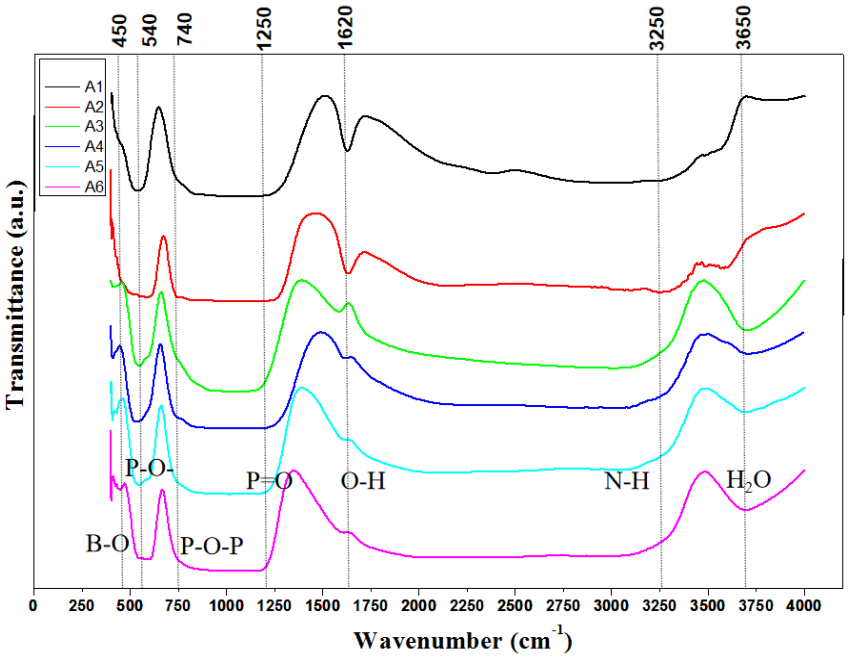

Fig. 2. The infrared spectra of $30P_2O_5$-$(50-x)SnF_2$-$xSnO$-$15WO_3$-$5B_2O_3$ glasses

The broad bands in the 2130-2300 cm^{-1} region, are ascribed to the CO_2 from the reducing atmosphere [29]. Similarly, the 3300 cm^{-1} bands are associated with N-H symmetrical stretching vibration belongs to the NH_3 [30], caused by the thermal decomposition of $NH_4H_2PO_4$, the bands at 3650-3750 cm^{-1} are ascribed to H_2O, which is attributed to the water-absorbing of Kbr during the infrared spectrum measurement.

3.1.3. XPS results

The chemical environment of elements in glass is a crucial evidence for structural discussion. Fig. 3a demonstrates the survey XPS spectra of PSWB glass from 0 to 1300 eV. The peak at 480 to 500 eV is assigned to the Sn 3d. The valence of Sn in glass could be two or four, that is, Sn (II) and Sn (IV). The Sn 3d energy level is usually divided into Sn $3d_{3/2}$ and Sn $3d_{5/2}$, and the binding energies distance of these two peaks can be authentication of the Sn valence. As revealed from Fig. 3b, the difference of Sn $3d_{3/2}$ and Sn $3d_{5/2}$ is 8.4 eV, which is similar to that of SnO_2. This result indicates that the Sn (IV) is the mainly chemical state in this PSWB glass.

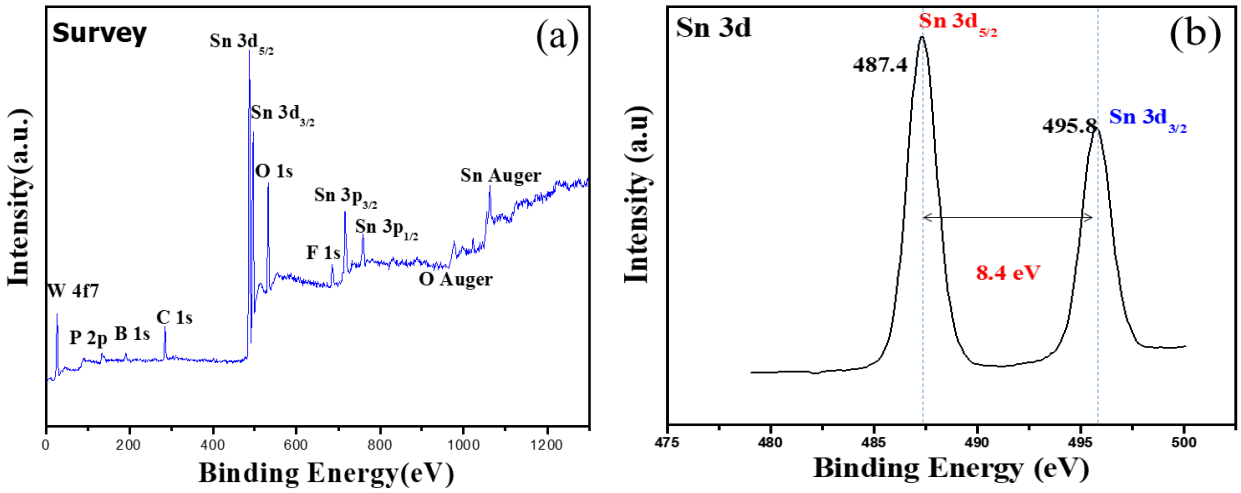

Fig. 3. (a) XPS survey spectra of PSWB glass; (b) Sn 3d XPS spectra of PSWB glasses

3.2. Glass properties

3.2.1. Density and electrical resistance

Density and electrical resistance of glass containing SnO (0-25 wt %) are demonstrated in Fig. 4. The density of pristine glass is 4.02 g/cm^3, as the SnO content gradually increase, glass density increases synchronously, the glass containing 25 wt% SnO is 4.65 g/cm^3, which mainly can be attributed to the partly replacement of SnF_2 by SnO. It has been reported [32] that the SnF_2 is volatile material, however, the SnO is stable in this PSWB glass system. Besides that, the electrical resistivity of glass tends to increase linearly, from 5.05*10^9 to 9.14*10^{11} Ω·cm, as the SnO content range from 0 to 25 wt %. The glass electrical resistance is determined by migration ability of metal ions [33]. In addtion, the Sn^{4+} contributes a lot to the electrical resistance in this PSWB system contain rich Sn. It has been noticed that the role of Sn played in glass network is both network former and modifier. The conclusion obtained from the infrared spectra reveals glass network becomes more cross-linked because of the increasing bridging oxygen number, which restrict the migration ability of Sn^{4+}, that is, more Sn interfere the glass network, then the change on glass electrical resistance could be explained.

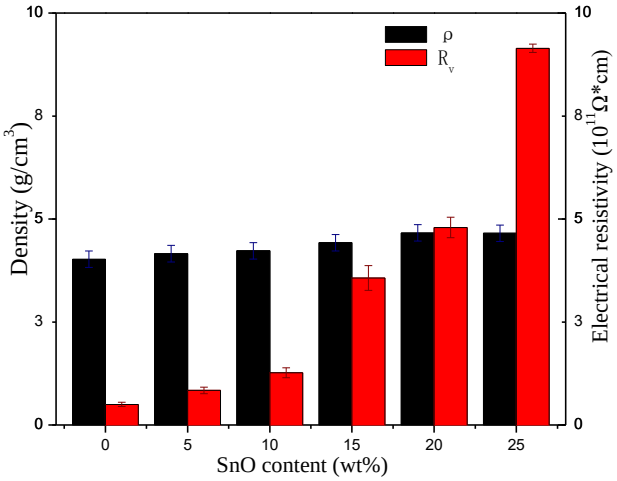

Fig. 4. The density (ρ) and electrical resistivity (R_v) of $30P_2O_5$-(50-x)SnF_2-xSnO-15WO_3-5B_2O_3 glasses

3.2.2. Thermal expansion curves

The TEC curves of glass contain SnO content (0 to 25 wt %) are shown in Fig. 5. Then the *CTE* and *Tg*, *Tf* are obtained. The *CTE* of 6 glass composition are 21.25*10^{-6} $^oC^{-1}$, 20.57*10^{-6} $^oC^{-1}$, 19.56*10^{-6} $^oC^{-1}$, 18.16*10^{-6} $^oC^{-1}$, 17.50*10^{-6} $^oC^{-1}$, 17.12*10^{-6} $^oC^{-1}$, respectively. The increasement in glass *CTE* indicates a denser glass structure and more difficult for glass to expand. The transition and diametric temperature increase from 85 ^oC to 110 ^oC, 103 ^oC to 125 ^oC, respectively. An accepted statement is that the thermal properties of glass are determined by its network structure [34]. The results in infrared spectra show that the length of phosphate chains shifts to longer, because the F at end of network is occupied by the BO, thus the tetrahedral units are more likely to connect with other group, which consequently improves the degree of polymerization of glass.

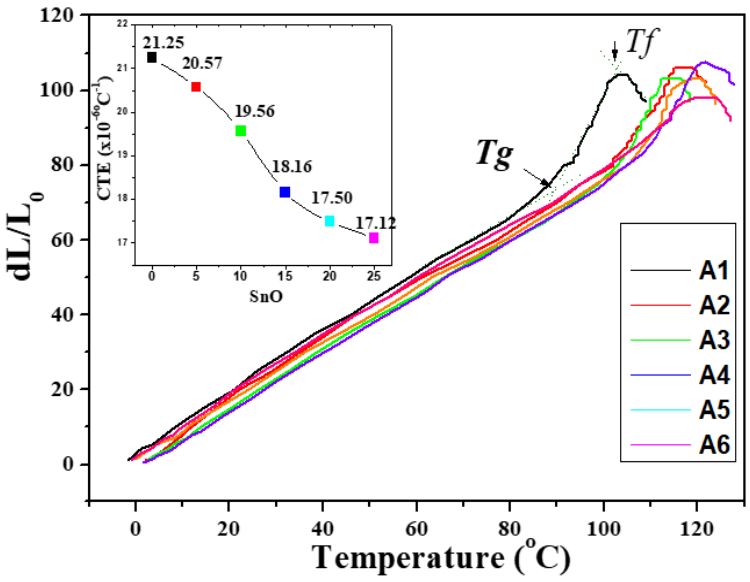

Fig. 5. The thermal expansion curves (TEC) of $30P_2O_5$-(50-x)SnF_2-xSnO-15WO_3-5B_2O_3 glasses

Table 1. Batch compositions and thermal properties of $30P_2O_5$-(50-x) SnF_2-xSnO-15WO_3-5B_2O_3 glasses

Sample ID	Composition (wt%)					*Tg* (±2°C)	*Tf* (±2°C)	*CTE* (10^{-6}/ °C)
	P_2O_5	SnF_2	SnO	WO_3	B_2O_3			
A1	30	50	0	15	5	85	103	21.25
A2	30	45	5	15	5	92	108	20.57
A3	30	40	10	15	5	96	112	19.56
A4	30	35	15	15	5	100	116	18.16
A5	30	30	20	15	5	103	118	17.50
A6	30	25	25	15	5	110	125	17.12

3.2.3. Water durability

Fig. 6 demonstrates the weight loss of these immersed glasses after immersing in the 60 °C for 48 hours, the weight loss is 8.5 wt %, then WL decreases to 1 wt % as the SnO content rises to 10 wt %. Moreover, there is almost no weight loss in glass contains 15 wt % SnO regardless of measuring error. To investigate the microstructure of glass, the immersed glass is examined using the SEM analysis, as shown in Fig. 7. A considerable number of fissures and pores cover the surface of the A1 sample, which is the pristine glass composition without SnO addition. The fluffy structure belongs to the A1 sample is caused by water erosion, the micropore on its surface is the water channel. With the increasing of SnO concentration, the proportion of crack and poles on surface decreases. On the surface of A4, A5, and A6, the structure tends to be smooth, indicating damage from the water gradually fade away, that is, the water durability of glass is remarkably enhanced by the addition of SnO.

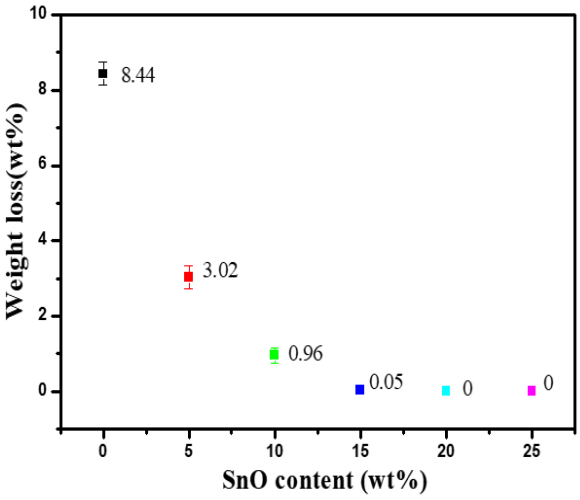

Fig. 6. The weight loss of $30P_2O_5$-(50-x)SnF_2-xSnO-15WO_3-5B_2O_3 glasses, after immersing in distilled water (60 °C, 48 hours)

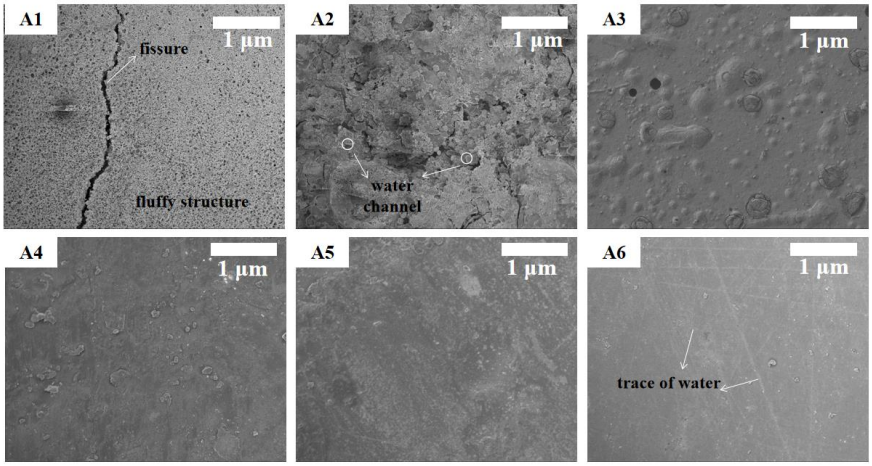

Fig. 7. The microstructure of $30P_2O_5$-(50-x) SnF_2-xSnO-15WO_3-5B_2O_3 glasses under the SEM analysis, after immersing in distilled water (60 ^oC, 48 hours)

The corrosion of phosphate glass by water is a complicated process [35]. H^+ from water or moisture tends to destroy the P=O double bond in the glass network, weakening the network bonding force and forming P-OH bonds [36], while its OH ions invade the glass network with that. Once the glass structure is ruined, water further erodes the glass, breaking the tetrahedron network. Eventually, the glass dissolves in water, and the neutral water becomes acidic owing to H^+ accelerated glass decomposition process [37]. However, as the infrared spectrum results reflect, the O-H bending vibration decreases and even vanish owing to the decreasing P=O vibration, then the glass structure not easy to be destroyed by the water. Instead, a more cross-linked network is formed, thus improving the water durability of glass.

3.2.4. Crystallization behavior and sealing performance

Considering practical applications, the sealant glass could be divided into crystalline or non-crystalline. The DSC result of A4 glass powder is shown in Fig. 8, no endothermic peaks are observed, indicating no crystal behavior happens during the melting process of glass powder. Then the melting temperature of glass powder is obtained to be about 295 ^oC. As revealed from the DSC results, the melting performance of glass powder was studied, as shown in Fig .9. Ten grams powder was pressed into the cylinder with a 12.7 mm diameter in a stainless mold. In order to reflect the melting process, five same powder columns were heated in the same condition. The powder cylinder comes to melt at about 200 ^oC, the cylinder shrinks to a black sphere at about 250 ^oC, then the shape tends to be half ball because of the gravity. It can be observed clearly that the contact angle becomes lower with the increasing temperature. As the temperature rises to 300 ^oC, the state of glass powder change from solid to vitreous state, the spreading area increases, which signify that the mobility of glass powder is ideal. No volatile matter was found on the surface, indicating the component of powder is stable and homogeneous.

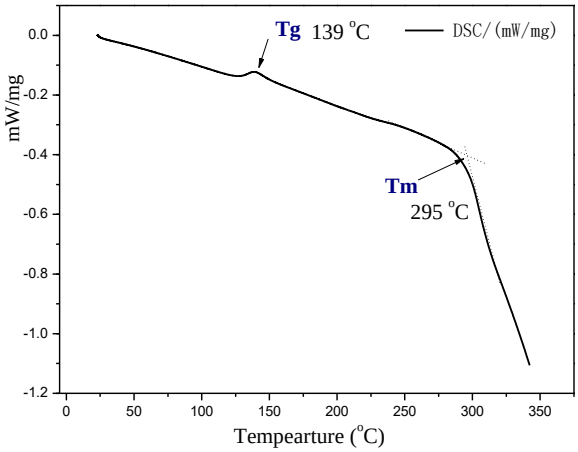

Fig. 8. The DSC result of the glass powder with composition of $30P_2O_5$-$35SnF_2$-$15SnO$-$15WO_3$-$5B_2O_3$ glass

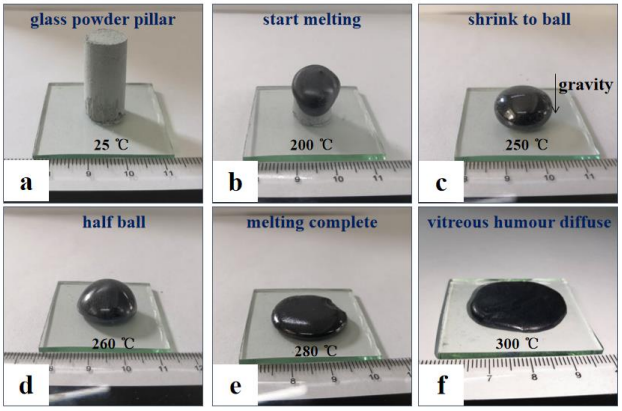

Fig. 9. The melting process of the glass powder with the $30P_2O_5$-$35SnF_2$-$15SnO$-$15WO_3$-$5B_2O_3$ composition

4. Conclusion

The $30P_2O_5$-$(50-x)SnF_2$-$xSnO$-$15WO_3$-$5B_2O_3$ ($0 \leq x \leq 25$ wt %) glass are prepared using the traditional melt quenching method. The T_g and T_f have an increase of 30 ^oC and the *CTE* decreases from 21.25 to $17.12*10^{-6}$ $^oC^{-1}$ as the SnO content increases up to 25 wt %. Besides that, the electrical resistivity rises to 10^{11} Ω·cm; the glass exhibits electrical insulating property. Additionally, the decrease in weight loss and SEM results indicate the glass water durability developed consequently with the increasing SnO concentration. At last, the melting performance of glass powder with 15 wt % SnO content reflects no crystallization and volatilization behavior, and the complete melting temperature is reached below 300 ^oC. This kind of P_2O_5-SnF_2-SnO-WO_3-B_2O_3 glass could be candidate material for low melting sealing applications.

Acknowledgments

This article is supported by the National Key Research and Development Program of China (No.2016YFB0303805), and the Jilin Scientific and Technological Development Program (No.20190302006GX).

References

[1] Y. He, D. Day, Glass Technol. **33**, 214 (1992).
[2] H. S. Liu, T. S. Chin, S. W. Yung, Materials Chemistry and Physics **50**, 1 (1997).
[3] M. T. Sebastian, R. Ubic, H. Jantunen, International Materials Reviews **60**(7), 392 (2015).
[4] G. Venkateswara Rao, H. D. Shashikala, Journal of Advanced Ceramics **3**, 109 (2014).
[5] X. Y. Zhang, W. Q. He, C. Li, H. Jiang, C. J. Li, L. Yu, Y. Shen, Advanced Materials Research **43-47**, 1030 (2014).
[6] T. Honma, J. Tatami, Materials Letters **160**, 375 (2015).
[7] J. Hong, D. Zhao, J. Gao, M. He, H. Li, G. He, Journal of Non-Crystalline Solids **356**(28-30), 1400 (2010).
[8] R. K. Brow, Journal of Non-Crystalline Solids **263-264**, 1 (2000).
[9] M. Sitarz, K. Bulat, Z. Olejniczak, Vibrational Spectroscopy **61**, 72 (2012).
[10] T. Y. Wei, Y. Hu, L. G. Hwa, Journal of Non-Crystalline Solids **288**(1-3), 140 (2001).
[11] M. S. Al Farisi, H. Hirano, S. Tanaka, Sensors and Actuators A: Physical **279**, 671 (2018).
[12] V. I. Malkovsky, S. V. Yudintsev, E. V. Aleksandrova, Journal of Nuclear Materials **508**, 212 (2018).
[13] N. Da, S. Krolikowski, K. H. Nielsen, J. Kaschta, L. Wondraczek, Journal of the American Ceramic Society **93**(8), 2171 (2010).
[14] N. Vedeanu, R. Stanescu, S. Filip, Journal of Non-Crystalline Solids **358**(16), 1881 (2012).
[15] M. Rajaram, D. E. Day, Journal of Non-Crystalline Solids **102**(1-3), 173 (1988).
[16] G. L. Paraschiv, F. Muñoz, G. Tricot, Journal of Non-Crystalline Solids **462**, 51 (2017).
[17] P. A. Tick, Phys. Chem. Glasses **25**(6), 149 (1984).
[18] T. Naito, A. Matsuda, D. Shiojiri et al., Journal of the Ceramic Society of Japan **121**(1413), 452 (2013).
[19] G.-S. Park, Y.-K. Kim, K.-K. Paek, J.-S. Kim, J.-H. Lee, B.-K. Ju, Electrochemical and Solid-State Letters **8**(12), G330 (2005).
[20] A. A. Ahmed, A. A. Ali, D. A. R. Mahmoud, A. M. El-Fiqi, Journal of Biomedical Materials Research Part A **98A**(1), 132 (2011).
[21] H. Takebe, Y. Baba, M. Kuwabara, Journal of Non-Crystalline Solids **352**(28-29), 3088 (2006).
[22] L. Cordeiro, R. M. Silva de Pietro, Journal of Non-Crystalline Solids **402**, 44 (2014).
[23] J. Y. Winegar, J. T. Harper, C. Brennan, J. Oelgoetz, A. Kovalskiy, Phys Procedia **44**, 159 (2013).
[24] C. Shaw, J. E. Shelby, Phys. Chem. Glass **29**, 87 (1988).
[25] Kevin Urman, Joshua U. Otaigbe Prog Polym. Sci. **32**, 1462 (2007).
[26] Y. M. Moustafa, K. El-Egili, Journal of Non-Crystalline Solids. **250**, 144 (1998).
[27] W. Hao, F. Li, Y. Ma et al., Materials Letters **236**, 506 (2019).
[28] L. N. Ignatieva, N. V. Surovtsev, V. G. Plotnichenko, Journal of Non-Crystalline Solids, **353**(13-15), 1238 (2007).
[29] D. Martín, P. Aparicio, Galán, Applied Clay Science **161**, 119 (2018).
[30] Y. Li, J. Yang, S. Xu, G. Wang, L. Hu, J. Mater. Sci. Technol. **21**(3), 391 (2005).
[31] Jiin-Jyh Shyu, Chih-Hsien Yeh, J. Mater. Sci. **42**, 4772 (2007).
[32] X. Li, Z. Xiao, M. Luo, X. Dong, T. Du, Y. Wang, Journal of Non-Crystalline Solids **469**, 62 (2017).
[33] A. El-Kheshen, C. Woda, M. Discher, Journal of Luminescence **200**, 254 (2018).
[34] S. N. S. Yaacob, Sahar, Solid State Sciences **81**, 51 (2018).
[35] J. Hong, D. Zhao, J. Gao, Journal of Non-Crystalline Solids **356**, 1400 (2010).
[36] F. Delahaye, L. Montagne, G. Palavit, Journal of Non-Crystalline Solids **242**(1), 25 (1998).
[37] P. Y. Shih, S. W. Yung, T. S. Chin, Journal of Non-Crystalline Solids **224**(2), 143 (1998).

*Corresponding author: zhengtao@cust.edu.cn